

Hierarchical Models: Intrinsic Separability in High Dimensions

Wen-Yan Lin

daniellin@smu.edu.sg

Abstract

It has long been noticed that high dimension data exhibits strange patterns. This has been variously interpreted as either a “blessing” or a “curse”, causing uncomfortable inconsistencies in the literature. We propose that these patterns arise from an intrinsically hierarchical generative process. Modeling the process creates a web of constraints that reconcile many different theories and results. The model also implies high dimensional data poses an innate separability that can be exploited for machine learning. We demonstrate how this permits the open-set learning problem to be defined mathematically, leading to qualitative and quantitative improvements in performance.

1. Introduction

Despite the wide-spread use of high dimensional data in computer vision and pattern recognition, understanding of high dimensions has proven elusive. In the dominant mathematical paradigm, high dimensions are “cursed”. The “curse” is rooted in a stochastic model where all instances are generated from some distribution-of-everything. This causes almost all instances to be equi-distant to any test point, making them indistinguishable from each other and any machine learning impossible [1, 2, 14].

Yet, effective high dimensional machine learning does exist. Further, it utilizes the same equations used to derive the “curse”. However, by assuming multiple generative distributions [34, 25, 42], the “curse” turns into a “blessing” that disentangles distribution instances. Both “curse” and “blessing” papers appear mathematically sound but their conclusions are contradictory and their assumptions are not mutually exclusive. This creates a puzzle.

We believe “curse” and “blessing” both stem from patterns arising from an intrinsically hierarchical data generation process. This would permit both their assumptions to be simultaneously true and may also explain why hierarchies are a recurring theme in language [38, 40], data-





				
Ours	bird: 0.999	horse: 0.861	airplane: 0.918	monkey: 0.945
	airplane: 0.001	dog: 0.125	bird: 0.070	dog: 0.051
	deer: 0.000	deer: 0.013	dog: 0.007	deer: 0.003
One-Class SVM	bird: 1.000	bird: 1.000	bird: 1.000	bird: 1.000
	dog: 0.000	dog: 0.000	dog: 0.000	dog: 0.000
	deer: 0.000	deer: 0.000	deer: 0.000	deer: 0.000

Figure 1: Our formulation permits multiple one-class learners to be fused into a multiclass classifier without re-training. This is not possible with traditional one-class frameworks [22] as demonstrated with one-class SVM [9], which assigns all images to the bird class.

structures [43] and clustering algorithms [41]. To understand this phenomenon, we develop a high dimensional *hierarchical-model*. The model unifies “curse” and “blessing” into an elegant web of constraints that links all generative distributions to each other and ultimately to a distribution-of-everything, forming an over-arching framework that reconciles many theories and results.

Beyond explanatory power, the *hierarchical-model* also predicts almost-all instances of a distribution and its sub-distributions, lie on a distinctive-shell that other instances almost-never enter. Such distinctive-shells can be estimated from instances of the distribution. This relates current observations to all other potential observations, creating a mathematical formulation for open-set learning!

Open-set learning is one of the most difficult machine learning problems. In it, a classifier trained on a small number of labeled classes must deal effectively with a much larger set of unlabeled classes [31, 45, 5]. Open-set learning is critical to handling unforeseen circumstances gracefully. However, it is relatively unstudied because, before the *hierarchical-model*, it appeared difficult (if not impossible) to make reasonable a priori assumptions on the properties of all possible unseen classes.

We formulate the classic open-set problem of one-class

learning in terms of the *hierarchical-model*. This creates a shell-learner that is algorithmically similar to one-class SVM [9]. However, unlike traditional one-class learning, it can approximate the absolute probability of a class given an image.

Such absolute scores are essential to operating in unknown environments. It also means scores of independently trained shell-learners can be combined coherently without re-training. This is especially important in life-long learning [22] where constant re-training can cause potentially catastrophic forgetting and interference problems [32]. An example is illustrated in Fig. 1.

In summary, this paper:

- Proposes a *hierarchical-model* that unifies “curse” and “blessing” approaches in high dimensions;
- Uses the *hierarchical-model* to predict the existence of distinctive-shells that make open-set problems amenable to mathematical analysis;
- Demonstrates a one-class learner which estimates the probability of a class given an image. Previously one-class learners only provided relative scores.

1.1. Related Works

This paper lies at the intersection of many research fields. Its formulation follows the long tradition of statistical machine learning. Examples include Expectation Maximization [13, 28, 12], Latent Dirichlet Allocation (LDA) [6, 35, 39], and Bayesian inference [7, 18, 17]. However, data density vanishes as dimensions increase, making probability density estimation ill-conditioned [36]. Thus, classic techniques often cannot scale to high dimensions. The *hierarchical-model* avoids this problem by focusing on distance relations rather than density.

While high dimensions are often mathematically intractable, computer vision has successfully utilized them in deep-learning. Examples include deep-learned image features [3, 21, 37], Generative Adversarial Networks [15, 20] and Variational Autoencoders [23]. Results are undoubtedly good but interpretation has proven difficult. We hope *hierarchical-models* make high dimensions and (indirectly) deep-learners more interpretable.

Finally, the *hierarchical-model* provides a statistical interpretation of high dimension Euclidean distances. As many data projection algorithms [33, 26, 27]) seek to minimize or preserve Euclidean distance, this has implications on the interpretation of their results as discussed in Sec. 7.2 of the supplementary.

2. Distributions in High Dimensions

Our approach is based on the analysis of high dimensional distributions. Following the definition in [25], a high dimensional distribution is one whose random vectors are

quasi-ideal, i.e. there are a large number of dimensions, most of whom are independent. This is elaborated below, with notations adapted from [25].

Definition 1.

- $d^2(\cdot)$ denotes an operator for normalized squared ℓ_2 norm, such that for $\mathbf{x} \in \mathbb{R}^k$, $d^2(\mathbf{x}) = \frac{\|\mathbf{x}\|^2}{k}$. If \mathbf{x} is the difference between two vectors, we refer to $d^2(\mathbf{x})$ as **normalized squared difference (NSD)**;
- $d(\cdot)$ is the normalized ℓ_2 norm operator, $d(\cdot) = \sqrt{d^2(\cdot)}$;
- $S(\boldsymbol{\mu}, r)$ denotes a thin shell centered at $\boldsymbol{\mu}$, with radius r .

Let $\mathbf{Z} = [\mathbf{Z}[1], \mathbf{Z}[2], \dots, \mathbf{Z}[k]]^T$ denote a k dimensional random vector where $\mathbf{Z}[i]$ is a random variable,

- \mathbf{Z} is **high dimensional** if and only if \mathbf{Z} is quasi-ideal [25], i.e., as dimension $k \rightarrow \infty$, each dimension $\mathbf{Z}[i]$ has finite fourth moment and a finite number of pairwise dependencies.
- $d^2(\cdot)$ operator can be applied to random vectors. $d^2(\mathbf{Z}) = \frac{\|\mathbf{Z}\|^2}{k}$ is a random variable formed by averaging \mathbf{z} 's squared elements;
- $\boldsymbol{\mu}_{\mathbf{Z}} = \mathbb{E}(\mathbf{Z}) = [\mathbb{E}(\mathbf{Z}[1]), \dots, \mathbb{E}(\mathbf{Z}[k])]^T$ is a vector of each dimension's expectation;
- $v_{\mathbf{Z}} = \sum_{i=1}^k \frac{\text{var}(\mathbf{Z}[i])}{k}$ is the average variance;
- $\stackrel{a.s.}{=}$ denotes almost-surely-equal. Thus, the relation $P(d(\mathbf{X} - \mathbf{c}) = t) \rightarrow 1$ as $k \rightarrow \infty$, is written $d^2(\mathbf{X} - \mathbf{c}) \stackrel{a.s.}{=} t$.

Unit-vector-normalization. As dimension $k \rightarrow \infty$, unit-vector-normalization causes individual entries to tend to 0. For unit-vector-normalized data, the definitions of $d^2(\cdot)$ and $v_{\mathbf{Z}}$ are modified to avoid dividing by k :

- $d^2(\cdot)$ is a squared ℓ_2 norm, such that $d^2(\mathbf{Z}) = \|\mathbf{Z}\|^2$;
- $v_{\mathbf{Z}} = \sum_{i=1}^k \text{var}(\mathbf{Z}[i])$, is the total variance.

Let \mathbf{A} and \mathbf{B} be two independent, high dimensional random vectors, with respective mean and average variances $\boldsymbol{\mu}_{\mathbf{A}}, \boldsymbol{\mu}_{\mathbf{B}}$ and $v_{\mathbf{A}}, v_{\mathbf{B}}$. Due to the law of large numbers, **the normalized squared difference between instances of \mathbf{A} and \mathbf{B} almost-surely depend, only on their mean and average variance [25]:**

$$d^2(\mathbf{A} - \mathbf{B}) \stackrel{a.s.}{=} v_{\mathbf{A}} + v_{\mathbf{B}} + d^2(\boldsymbol{\mu}_{\mathbf{A}} - \boldsymbol{\mu}_{\mathbf{B}}). \quad (1)$$

This is key to understanding high dimensions.

Replacing \mathbf{B} in Eq. (1) by a distribution of mean \mathbf{c} and zero variance, yields

$$d^2(\mathbf{A} - \mathbf{c}) \stackrel{a.s.}{=} v_{\mathbf{A}} + d^2(\boldsymbol{\mu}_{\mathbf{A}} - \mathbf{c}), \quad \forall \mathbf{c} \in \mathbb{R}^k. \quad (2)$$

Let the **distribution-of-everything** represent a hypothetical, generative distribution that fully explains the creation of all natural images. If \mathbf{A} represents the distribution-of-everything, Eq. (2) means almost-all instances are equidistant to any point \mathbf{c} . This has been used to argue that high-dimensions are “cursed” as it supposedly makes instances indistinguishable from each other [2]. If true, the

“curse” implies no machine learning algorithm can work in high dimensions. However, if we consider a more complex hierarchical generative model, the conclusion changes.

Our *hierarchical-model* is based on three assumptions: 1) Images are instances of some generative distribution; 2) Generative distributions are high dimensional; 3) Except for the distribution-of-everything, each generative distribution is a sub-distribution of some parent.

The “curse” does not directly apply to *hierarchical-models* as it cannot account for pairwise distances between instances of the same sub-distribution. This is because Eq. (2)’s almost-sure-equality permits exceptional events of infinitesimally small probability. Thus if each sub-distribution \mathbf{A}_θ accounts for only an infinitesimal fraction of \mathbf{A} ’s instances, the pairwise distance between its instances could be exceptional.

While specific sub-distributions may violate Eq. (2), in aggregate, they must conform to Eq. (2). This creates a web of constraints linking all generative distributions (and images) to each other and to the distribution-of-everything.

3. The Hierarchical-Model

We begin by defining the relation between a distribution and its sub-distributions. The definition is then applied recursively to create the *hierarchical-model*.

Let \mathbf{A} be a high-dimensional random vector with probability density function $f_{\mathbf{A}}(\mathbf{a})$, which represents a distribution-of-everything. $f_{\mathbf{A}}(\mathbf{a})$ is a compound distribution, i.e., it is distributed according to some sub-distributions, with these distributions’ parameters themselves being random variables. $\Theta = \{V_\Theta, \mathbf{M}_\Theta, \dots, \text{other parameters}\}$ is a set of random vectors representing sub-distribution parameters. V_Θ and \mathbf{M}_Θ represent the average variance and mean parameters respectively. We write $\mathbf{A} = \mathbf{A}_\Theta$ to denote that parent distribution \mathbf{A} is explained by its sub-distribution parameters Θ such that:

$$f_{\mathbf{A}}(\mathbf{a}) = f_{\mathbf{A}_\Theta}(\mathbf{a}) = \int_{-\infty}^{\infty} f_{\Theta}(\theta) f_{\mathbf{A}|\Theta}(\mathbf{a}|\theta) d\theta. \quad (3)$$

where each sub-distribution is itself high-dimensional¹.

Let \mathbf{a}_θ be an instance of \mathbf{A}_θ , it is generated by a two-step process: 1) Generate an instance of sub-distribution parameters θ from Θ . The random vector associated with θ is \mathbf{A}_θ ; 2) Generate instance \mathbf{a}_θ from \mathbf{A}_θ .

We recursively define sub-distributions of sub-distributions through a hierarchical random process

$$\mathbf{A}_{\Theta^n} = (((\mathbf{A}_{\Theta^{[0]}})_{\Theta^{[1]}})_{\Theta^{[2]}})_{\Theta^{[3]}} \dots)_{\Theta^{[n]}} = \mathbf{A},$$

¹An example is compounding a Gaussian distribution with mean distributed according to another Gaussian distribution. Let each dimension of \mathbf{A} be independently distributed with $\mathbf{A}[i] \sim N(\mathbf{M}[i], \sigma_1^2)$, $\mathbf{M}[i] \sim N(\mu[i], \sigma_2^2)$. The parameters of \mathbf{A} are $\mu_{\mathbf{A}} = \mu$, $v_{\mathbf{A}} = \sigma_1^2 + \sigma_2^2$.

where operator $\Theta^{[i]}$ represents the random sampling of a sub-distribution, which in turn forms the parent distribution for $\Theta^{[i+1]}$. \mathbf{A}_{Θ^n} denotes an n level hierarchical-process, with $\mathbf{A}_{\Theta^{[0]}} = \mathbf{A}$.

If \mathbf{A}_{Θ^n} and \mathbf{A}_{Θ^m} denote independent runs of a hierarchical-process, starting from \mathbf{A} , from Eq. (1),

$$d^2(\mathbf{A}_{\Theta^n} - \mathbf{A}_{\Theta^m}) \stackrel{a.s.}{=} d^2(\mathbf{A} - \mathbf{A}) \stackrel{a.s.}{=} 2v_{\mathbf{A}}, \quad m, n \in \mathbb{Z}_0^+. \quad (4)$$

The instantiated sub-distribution parameters of a hierarchical-process are denoted as

$$\theta^n = \theta^{[0]} \theta^{[1]} \theta^{[2]} \dots \theta^{[n]},$$

where $\theta^{[0]}$ is the parameter of \mathbf{A} . θ^n records the distribution parameters’ values at every level, until the final distribution \mathbf{A}_{θ^n} . Since the final random vector is completely characterized by the final distribution parameters, $\mathbf{A}_{\theta^n} = \mathbf{A}_{\theta^{[n]}}$.

A *hierarchical-model* is a series of hierarchical processes, where at any i^{th} stage, the \mathbf{A}_{θ^i} random vector can be a parent of multiple, new hierarchical processes.

In the *hierarchical-model*, any two data-points are instantiations of two independent hierarchical-processes starting from some, most recent common ancestor. Let \mathbf{A}_{θ^n} denote their common ancestor and $\mathbf{A}_{\theta^n \Theta^i}$, $\mathbf{A}_{\theta^n \Theta^j}$ their distributions. From Eq. (4), the normalized squared difference (NSD) between any two instances is:

$$d^2(\mathbf{A}_{\theta^n \Theta^i} - \mathbf{A}_{\theta^n \Theta^j}) \stackrel{a.s.}{=} 2v_{\theta^{[n]}}, \quad \forall i, j, n \in \mathbb{Z}_0^+. \quad (5)$$

This is summarized in Theorem 1.

Theorem 1. (Pairwise Difference) *The hierarchical-model predicts that normalized difference between any two data-points is almost-surely $\sqrt{2v}$, where v is the average variance of their most recent common ancestor distribution.*

Figure 2 illustrates a numerical example of the pairwise NSD. Similar to the “curse” [2], this formulation begins with a distribution-of-everything. However, the NSD is not a constant. Instead, there is a defined pattern of distances which algorithms can exploit as a “blessing”. The distance patterns also ensure Euclidean distance remains meaningful in high dimensions, as elaborated in the supplementary.

In practice, NSD is very often equal to $2v_{\mathbf{A}}$ as the most recent common ancestor is often the distribution-of-everything. This creates a paradox in which algorithms working directly with the affinity matrix experience a “curse” but those dealing with nearest-neighbor distance do not.

3.1. Parameter Constraints

This subsection relates distribution parameters across different hierarchies of the *hierarchical-model*, creating the key constraints exploited in later sections.

Thus far, a sub-distribution with identical parameters to its parent is considered valid. Without loss of generality, we

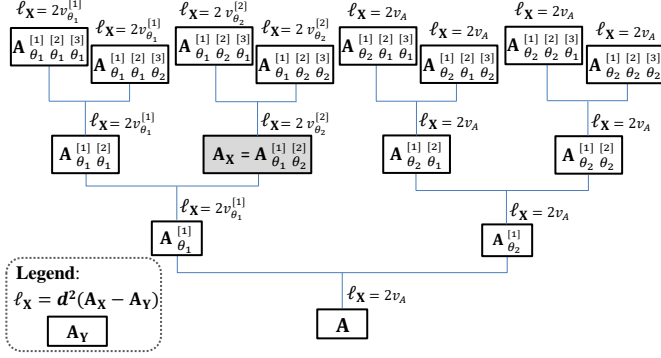


Figure 2: A hierarchical-model with \mathbf{A} as distribution-of-everything. \mathbf{A}_Y refers to the random vector enclosed by a rectangle. Normalized squared difference between \mathbf{A}_Y and the reference random vector, \mathbf{A}_X , is denoted by ℓ_X . From Eq. (5), ℓ_X is almost-surely 2 times the average variance of their most recent common ancestor. Each path from root to leaf, represents a hierarchical-process.

define a non-trivial hierarchical-process as one where sub-distributions almost-surely have, finite difference in either mean or average variance, from its immediate parent:

$$p(V_{\Theta}^{[i+1]} = V_{\Theta}^{[i]}) = 0$$

$$\text{or } p(d^2(\mathbf{M}_{\Theta}^{[i+1]} - \mathbf{M}_{\Theta}^{[i]}) = 0) = 0, \quad \forall i \in \mathbb{Z}_0^+. \quad (6)$$

A non-trivial *hierarchical-model* is one where all hierarchical-processes are non-trivial.

For sub-distribution $\mathbf{A}_{\theta^n} = \mathbf{A}_{\theta[n]}$, its mean and average variance are denoted as $\mu_{\theta[n]}$, $v_{\theta[n]}$ respectively. The mean and average variance of its hierarchical process descendants are denoted by random variables $\mathbf{M}_{\theta^n \Theta^j}$, $V_{\theta^n \Theta^j}$.

Theorem 2. (Mean-Variance Constraint) *The mean and average variance of distributions generated by a hierarchical process with \mathbf{A}_{θ^n} as parent must adhere to the constraint:*

$$V_{\theta^n \Theta^j} + d^2(\mathbf{M}_{\theta^n \Theta^j} - \mu_{\theta[n]}) \stackrel{a.s.}{=} v_{\theta[n]}, \quad \forall n, j \in \mathbb{Z}_0^+. \quad (7)$$

Proof. Recall that $\mathbf{A}_{\theta^n \Theta^j} = \mathbf{A}_{\theta^n}$. Thus, by requiring the sub-distributions to, in aggregate, conform to the almost-surely constraint of their parent, using Eq. (2) yields:

$$d^2(\mathbf{A}_{\theta^n \Theta^j} - \mu_{\theta[n]}) \stackrel{a.s.}{=} d^2(\mathbf{A}_{\theta^n} - \mu_{\theta[n]}) \stackrel{a.s.}{=} v_{\theta[n]},$$

$$\stackrel{a.s.}{=} V_{\theta^n \Theta^j} + d^2(\mathbf{M}_{\theta^n \Theta^j} - \mu_{\theta[n]}) \quad (8)$$

□

Corollary 1. *Distributions derived from a non-trivial hierarchical-process starting at \mathbf{A}_{θ^n} , almost-surely have average variances less than $v_{\theta[n]}$. i.e.,*

$$V_{\theta^n \Theta^j} \stackrel{a.s.}{<} v_{\theta[n]}, \quad \forall j, n \in \mathbb{Z}_0^+. \quad (9)$$

That is, if $\theta^{[i]}$ and $\theta^{[j]}$ are distribution parameters from the same non-trivial hierarchical-process, almost-surely,

$$v_{\theta^{[i]}} > v_{\theta^{[j]}}, \quad \forall i < j, i, j \in \mathbb{Z}_0^+.$$

Proof. This follows from Theorem 2 and Eq. (6). □

Manipulating Eq. (2), Theorem 2 and Corollary 1 leads to distinctive-shells, the paper's main result.

3.2. Distinctive-Shells

Consider a non-trivial hierarchical-process that starts from the distribution-of-everything, \mathbf{A} and terminates at \mathbf{A}_{θ^n} . Instances of \mathbf{A}_{θ^n} and all its sub-distributions, $\mathbf{A}_{\theta^n \Theta^j}$ are labeled α .

From Eq. (2), $\forall \mathbf{c} \in \mathbb{R}^k$

$$d^2(\mathbf{A}_{\theta^n \Theta^j} - \mathbf{c}) \stackrel{a.s.}{=} d^2(\mathbf{A}_{\theta^n} - \mathbf{c}) \stackrel{a.s.}{=} v_{\theta[n]} + d^2(\mu_{\theta[n]} - \mathbf{c}). \quad (10)$$

Thus instances of α , are almost-always members of the set of shells, $\{\mathcal{S}(\mathbf{c}, \sqrt{v_{\theta[n]} + d^2(\mu_{\theta[n]} - \mathbf{c})}) \mid \mathbf{c} \in \mathbb{R}^k\}$. The minimum radius shell, $\mathcal{S}(\mu_{\theta[n]}, \sqrt{v_{\theta[n]}})$, is termed the **distinctive-shell** and is of unique significance.

We represent the ancestors of \mathbf{A}_{θ^n} as \mathbf{A}_{θ^m} , $m < n$. All possible non- α instances can be represented by $\mathbf{A}_{\theta^m \Theta^i}$. Equation (2) relates all such instances to $\mu_{\theta[n]}$ through

$$d^2(\mathbf{A}_{\theta^m \Theta^i} - \mu_{\theta[n]}) \stackrel{a.s.}{=} d^2(\mathbf{A}_{\theta^m} - \mu_{\theta[n]})$$

$$\stackrel{a.s.}{=} v_{\theta[m]} + d^2(\mu_{\theta[m]} - \mu_{\theta[n]}). \quad (11)$$

From Theorem 2, almost-surely,

$$v_{\theta[n]} + d^2(\mu_{\theta[m]} - \mu_{\theta[n]}) = v_{\theta[m]}, \quad \forall m < n, m, n \in \mathbb{Z}_0^+. \quad (12)$$

Combining Eq. (12) and Eq. (11), almost-surely,

$$d^2(\mathbf{A}_{\theta^m \Theta^i} - \mu_{\theta[n]}) \stackrel{a.s.}{=} 2v_{\theta[m]} - v_{\theta[n]}, \quad \forall m < n, m, n \in \mathbb{Z}_0^+. \quad (13)$$

Thus for each \mathbf{A}_{θ^m} ancestor of \mathbf{A}_{θ^n} , Corollary 1 almost-surely implies

$$d^2(\mathbf{A}_{\theta^0 \Theta^i} - \mu_{\theta[n]}) \stackrel{a.s.}{>} d^2(\mathbf{A}_{\theta^1 \Theta^i} - \mu_{\theta[n]}) \stackrel{a.s.}{>} \dots$$

$$\stackrel{a.s.}{>} d^2(\mathbf{A}_{\theta^n \Theta^i} - \mu_{\theta[n]}) \stackrel{a.s.}{=} v_{\theta[n]}. \quad (14)$$

Recall that $\mathbf{A}_{\theta^m \Theta^i}$ represents all possible non- α instances. Thus Eq. (14) guarantees non- α instances almost-surely fall outside the distinctive-shell. Further, Eq. (10) enables us to estimate the distinctive-shell by fitting the tightest possible shell to instances of α . This makes it possible to algorithmically relate current observations with all other potential observations!

4. Shell Based Learning

This section applies the theory of distinctive-shells to practical open-set problems, where a concept detector trained on limited data must generalize to unknown environments.

4.1. Formulation

Unit-Vector-Normalization

Despite the complexity of the image formation process, generative distributions of digital images cannot be modeled as high dimensional. This is because the brightness of all pixels in an image is correlated by a common exposure setting, making dimensions dependent. Exposure induced scaling can be removed by unit-vector-normalization that divides each data point by its ℓ_2 norm, converting all data to unit vectors.

Suppose \mathbf{A} is a *hierarchical-model's* distribution-of-everything. If each \mathbf{a}_i instance, is perturbed by a random scalar such that $\tilde{\mathbf{a}}_i = s_i \mathbf{a}_i$, after unit-vector-normalization, $\frac{\tilde{\mathbf{a}}_i}{\|\tilde{\mathbf{a}}_i\|} = \frac{\mathbf{a}_i}{\|\mathbf{a}_i\|}$, which is identical to unit vector normalization on the un-perturbed instances. Thus, the effect of normalization of perturbed instances can be understood by analyzing the normalization of un-perturbed instances.

Setting \mathbf{c} to a zero vector, $\mathbf{0}$, in Eq. (2) yields

$$d^2(\mathbf{A}_{\Theta^n}) \stackrel{a.s.}{=} d^2(\mathbf{A}) \stackrel{a.s.}{=} v_{\mathbf{A}} + d^2(\boldsymbol{\mu}_{\mathbf{A}}) = \lambda_{\mathbf{A}}, \quad (15)$$

where $\lambda_{\mathbf{A}}$ is a constant. Thus, unit-vector-normalization of *hierarchical-model* data, is almost-surely equivalent to scaling the entire *hierarchical-model* by a constant factor.

From the definition of $d^2(\cdot)$ and Eq. (15),

$$d^2(\mathbf{A}) = \frac{\|\mathbf{A}\|^2}{k} \stackrel{a.s.}{=} \lambda_{\mathbf{A}} \Rightarrow \|\mathbf{A}\| \stackrel{a.s.}{=} \sqrt{\lambda_{\mathbf{A}} k}, \quad (16)$$

where k is the number of dimensions. If $\hat{\mathbf{A}}$ be the normalized version of \mathbf{A} , after normalization, $\|\hat{\mathbf{A}}\|^2 \stackrel{a.s.}{=} \frac{\|\mathbf{A}\|^2}{\lambda_{\mathbf{A}} k}$. Since k is already part of this normalization, for post unit-vector-normalized data, we modify the definition of $d^2(\cdot)$ and v operators, detailed in Sec. 2, to avoid another division by k . This extends all previous high dimensional analysis to post unit-vector-normalized data.

Statistical Framework

Let $\mathbf{x} \in \mathbb{R}^k$ be a data point and $y \in \mathbb{Z}_0^+$ some label. The goal of learning is to estimate $p(y|\mathbf{x})$ for all y and \mathbf{x} .

If instances of a $\mathbf{A}_{\Theta^n \Theta^i}$ correspond to label α , from Eq. (14), α instances almost-surely lie on distinctive-shell $\mathcal{S}(\boldsymbol{\mu}_{\Theta^n}, \sqrt{v_{\Theta^n}})$, which exclude almost-all other instances. Thus, if \mathbf{x} is modified to be the distance from the distinctive-shell, we have the following:

$$\begin{aligned} p(y = \alpha | \mathbf{x} = 0) &= 1, & p(\mathbf{x} = 0 | y = \alpha) &= 1 \\ p(y \neq \alpha | \mathbf{x} = 0) &= 0, & p(\mathbf{x} = 0 | y \neq \alpha) &= 0 \\ p(y = \alpha | \mathbf{x} \neq 0) &= 0, & p(\mathbf{x} \neq 0 | y = \alpha) &= 0 \\ p(y \neq \alpha | \mathbf{x} \neq 0) &= 1, & p(\mathbf{x} \neq 0 | y \neq \alpha) &= 1 \end{aligned} \quad (17)$$

This can be summarized as $p(y = \alpha | \mathbf{x}) = p(\mathbf{x} | y = \alpha)$. In practice, we use:

$$p(y = \alpha | \mathbf{x}) \approx p(\mathbf{x} | y = \alpha). \quad (18)$$

While Eq. (18) does not represent all perturbations, it is still a remarkable approximation as it frees us from assuming a prior (that most statistical formulations require). This is key to permitting open-set formulations for unknown operating environments.

Shell Fitting

Given l instances of class α , $\{\mathbf{f}_0, \mathbf{f}_1, \dots, \mathbf{f}_l\}$, from Eq. (14), the distinctive-shell $\mathcal{S}(\boldsymbol{\mu}_{\Theta^n}, \sqrt{v_{\Theta^n}})$ is estimated by minimizing

$$\arg \min_{\{\boldsymbol{\mu}, v\}} \frac{1}{l} \sum_{i=1}^l \|\mathbf{f}_i - \boldsymbol{\mu}\|^2 - v\|^2 + \lambda \|\boldsymbol{\mu}\|^2. \quad (19)$$

$\boldsymbol{\mu}, v$ are the respective estimates of $\boldsymbol{\mu}_{\Theta^n}, v_{\Theta^n}$ and λ is a regularizer that encourages small shells. Let $\mathbf{x}_i = \|\mathbf{f}_i - \boldsymbol{\mu}\|^2$. $p(\mathbf{x}|\alpha)$ is estimated by applying a parzen window to \mathbf{x}_i instances. This approximates $p(\alpha|\mathbf{x})$ in Eq. (18).

Note: One-class SVM libraries [9] can also estimate $\boldsymbol{\mu}$ but minimizing Eq. (19) is better in extreme cases, as shown in supplementary Sec. 8.3.

4.2. Re-normalization

This section shows the impact of coordinate frame choice on learning. We assume data is unit-vector-normalized.

Similar to Sec. 3.2, let \mathbf{A}_{Θ^m} be some ancestor distribution of \mathbf{A}_{Θ^n} . From Eq. (13), the gap in distinctive-shell distance between instances of $\mathbf{A}_{\Theta^m \Theta^i}$ and α instances of $\mathbf{A}_{\Theta^n \Theta^j}$ is:

$$\begin{aligned} G_{mn} &= d^2(\mathbf{A}_{\Theta^m \Theta^i} - \boldsymbol{\mu}_{\Theta^n}) - d^2(\mathbf{A}_{\Theta^n \Theta^j} - \boldsymbol{\mu}_{\Theta^n}) \\ &\stackrel{a.s.}{=} 2(v_{\Theta^m} - v_{\Theta^n}), \quad m \leq n. \end{aligned} \quad (20)$$

For convenience, we shorten the expression to

$$g_{mn} = 2(v_{\Theta^m} - v_{\Theta^n}), \quad m \leq n. \quad (21)$$

In theory, a finite gap suffices for separability. However, due to noise, ensuring the largest possible gap is important. Gaps can be altered through **re-normalization**, where each dimension is translated by some value and resultant vectors unit-normalized again to magnitude 1.

Given the mean of the distribution-of-everything, $\boldsymbol{\mu}_{\mathbf{A}}$, we can re-normalize by subtracting $\boldsymbol{\mu}_{\mathbf{A}}$ from all instances and dividing by their new magnitude. From Eq. (2), $d^2(\mathbf{A}_{\Theta^k} - \boldsymbol{\mu}_{\mathbf{A}}) \stackrel{a.s.}{=} v_{\mathbf{A}}$. Thus this step is equivalent to re-centering almost-all instances and dividing them by a scalar $s_{\mathbf{A}} = \sqrt{v_{\mathbf{A}}}$. Let $\tilde{\mathbf{A}}_{\Theta^m \Theta^i}, \tilde{\mathbf{A}}_{\Theta^n \Theta^j}$ be the re-normalized sub-distributions. The gap becomes:

$$\widetilde{g_{mn}} = \frac{2(v_{\Theta^m} - v_{\Theta^n})}{s_{\mathbf{A}}^2} = \frac{2(v_{\Theta^m} - v_{\Theta^n})}{v_{\mathbf{A}}}, \quad m \leq n. \quad (22)$$

As data has been unit-vector-normalized, $d^2(\mathbf{A} - \mathbf{0}) \stackrel{a.s.}{=} v_{\mathbf{A}} + d^2(\boldsymbol{\mu}_{\mathbf{A}} - \mathbf{0}) = 1$ and $v_{\mathbf{A}} \leq 1$. Thus re-normalizing with $\boldsymbol{\mu}_{\mathbf{A}}$ is guaranteed to not reduce the gap. If $\boldsymbol{\mu}_{\mathbf{A}}$ is far from zero, $v_{\mathbf{A}}$ can be very small, causing a corresponding huge improvement in the gap for almost-all pairs of distributions m, n . Re-normalization with $\boldsymbol{\mu}_{\mathbf{A}}$ is identical to standard normalization procedures in machine learning and helps explain the importance of this step in general machine-learning.

The gap can be further manipulated if we have knowledge of the ancestors of \mathbf{A}_{θ^n} . This is summarized as:

Corollary 2. (*Re-Normalization*) Let \mathbf{A}_{θ^l} be some ancestor of \mathbf{A}_{θ^n} , i.e. $l \in \mathbb{Z}_0^+, l \leq n$. If we re-normalize data with $\boldsymbol{\mu}_{\theta^l}$, almost-surely,

$$\widetilde{g}_{mn} = \begin{cases} \frac{2(v_{\theta^{[m]}} - v_{\theta^{[n]}})}{v_{\theta^{[l]}}}, & \text{if } 0 \leq l \leq m \leq n, \\ \frac{2(v_{\theta^{[l]}} - v_{\theta^{[n]}})}{v_{\theta^{[l]}}}, & \text{if } 0 \leq m \leq l \leq n. \end{cases} \quad (23)$$

Proof. Proof is in Sec. 7.1 of the supplementary.

From Corollary 1,

$$1 \geq v_{\mathbf{A}} > v_{\theta^1} > v_{\theta^2} > v_{\theta^3} \dots > v_{\theta^n}.$$

Thus, the first case of Eq. (23) implies for instances of $\mathbf{A}_{\theta^m \ominus \theta^j}$, where m is between l and n , re-normalizing with $\boldsymbol{\mu}_{\theta^{[l]}}$, increases separability from instances of $\mathbf{A}_{\theta^n \ominus \theta^j}$ which correspond to class α . The second case of Eq. (23) shows this comes at the expense of separability when m is less than l . This is equivalent to stretching contrast (separation gap) of \mathbf{A}_{θ^l} descendants at the expense of compressing contrast of its ancestors. In the extreme case, where $l = n$, the gap between \mathbf{A}_{θ^n} and all its ancestors vanishes. Thus, standard normalization with one-class learning causes disastrously bad results, as shown in supplementary Sec. 8.2.

These trade-offs motivate Sec. 4.4’s training of a stack of one-class learners by re-normalizing data with different ancestor means. This enables the exceptionally fine retrieval demonstrated in Fig. 4.

4.3. Magic of Deep Learned Features

Using deep-learned features is known to “magically” improves learning results. This phenomenon can be studied in the context of *hierarchical-models*.

Part of the improvement may arise from an innately better representation (that we cannot explain), which reduces the ratio of within-class variance to between-class variance, essentially amplifying the gap in Eq. (23).

However, Sec. 4.2 shows coordinate frame choice is also important to learning. In particular, it is ideal if the mean of the distribution-of-everything is at $\mathbf{0}$. Deep-learned do indeed seem to have made this choice and changing their coordinate frame significantly reduces performance, as shown

in Sec. 8.4 of the supplementary. We also leverage this property in our one-class learning algorithm in Sec. 4.4.

4.4. Implementation

We term our overall algorithm **Shell-Stacked (SS)**. Details are as follows.

Training (Algorithm 1): Given training images from a target class α , we store their unit-vector-normalized ResNet features [21] as \mathbf{F} . Optionally, we are given a set of ancestor distribution means or “external knowledge”, denoted as $\mathbf{M} = [\mathbf{m}_1, \mathbf{m}_2, \dots, \mathbf{m}_K]$. If \mathbf{M} is not given, we estimate it by crawling $K - 1$ semantic concepts related to the target class α from the Internet. We first estimate the mean, \mathbf{m} of training data \mathbf{F} . For crawled concepts, we compute the mean of their image features and rank them from nearest to furthest from \mathbf{m} , creating $[\widetilde{\mathbf{m}}_1, \widetilde{\mathbf{m}}_2, \dots, \widetilde{\mathbf{m}}_{K-1}]$. By taking a weighted average of \mathbf{m} with $\widetilde{\mathbf{m}}_i$, we estimate \mathbf{m}_i , an approximation of a parent distribution mean. This is given by $\mathbf{m}_i = \frac{\mathbf{m} + \sum_{j=1}^i \widetilde{\mathbf{m}}_j}{i+1}$, $i \geq 1$, $\mathbf{m}_K = \mathbf{0}$. The final zero vector corresponds to assuming ResNet feature’s distribution-of-everything has mean, $\mathbf{0}$, as described in Sec. 4.3.

If internet crawling is unavailable, set $\mathbf{M} = [\mathbf{0}]$. This is termed **Shell-One (SO)** and is a special case of SS.

We re-normalize all input data with each \mathbf{m}_i and fit a tight shell to the re-normalized data, using Eq. (19), to estimate shell centers, $\boldsymbol{\mu}_i$ and probability density function $p_i(\mathbf{x}_i = x_i | \alpha)$. The output is a list parameters $\mathbf{m}_i, \boldsymbol{\mu}_i$ and p_i .

Testing (Algorithm 2): \mathbf{y} is a unit-normalized ResNet feature. Compute $\widetilde{\mathbf{y}}_i$ by re-normalizing \mathbf{y} with \mathbf{m}_i . The score of \mathbf{y} is $\frac{1}{K} \sum_{i=1}^K p_i(d^2(\boldsymbol{\mu}_i - \widetilde{\mathbf{y}}_i) | \alpha)$.

4.5. Errors in Shell Learning

In theory, shell fitting results should be perfect. In practice, there are three major error sources:

Firstly, computationally tractable features do not have infinite dimensions, with even deep-learned features having only a few hundred linearly independent dimensions. Thus data typically form cloudy approximates of the ideal shell;

Secondly, there can be semantic gaps between labels and distributions. An extreme example would be the label apple mapping to both the iPhone and the fruit. This causes an excessively large common shell that encompasses many unrelated instances. The problem can be alleviated by clustering. However, that is beyond this paper’s scope;

Thirdly, while Eq. (19)’s regularization provides robustness its estimated shells are too small, causing some true instances to fall outside the shell.

5. Experiments

This section focuses on checking the *hierarchical-model’s* predictions and quantitative analysis of shell based learning.

```

Input: 1) Training features  $\mathbf{F} = [\mathbf{f}_1, \mathbf{f}_2, \dots, \mathbf{f}_N]$ ;
        2) (optional) "External knowledge" of ancestor distributions
        mean  $\mathbf{M} = [\mathbf{m}_1, \mathbf{m}_2, \dots, \mathbf{m}_K]$ 
1 S = empty list;
2 for  $i = 1$  to  $K$  do
3    $\widetilde{\mathbf{F}}_i = \text{UNIT-VECTOR-NORM}(\mathbf{F} - \mathbf{m}_i)$  # re-normalize;
4    $\boldsymbol{\mu}_i = \text{SHELL-FIT}(\widetilde{\mathbf{F}})$  # estimate shell-center with Eq.(19);
5    $\mathbf{X}_i = \{\mathbf{x}_j | \mathbf{x}_j = \|\widehat{\mathbf{f}}_{ij} - \boldsymbol{\mu}_i\|^2\}$ , where  $\widehat{\mathbf{f}}_{ij} = \widetilde{\mathbf{F}}_i[:, j]$ ;
        #  $\mathbf{x}_j$  represents distance from shell-center;
6    $p_i(\mathbf{x}) = \text{DENSITY-ESTIMATION}(\mathbf{X}_i)$ ;
7   S.append( $[\mathbf{m}_i, \boldsymbol{\mu}_i, p_i(\mathbf{x})]$ );
8 return S

```

```


Input: 1) Test feature  $\mathbf{f}$ ; 2) Distinctive-shells of  $\alpha$ ,
 $\mathbf{S} = [\mathbf{s}_1, \mathbf{s}_2, \dots, \mathbf{s}_K]$ .
1  $y = 0$ ;
2 for  $i = 1$  to  $K$  do
3    $[\tilde{\mathbf{m}}_i, \boldsymbol{\mu}_i, p_i(\mathbf{x})] = \mathbf{s}_i$ ;
4    $\tilde{\mathbf{f}}_i = \text{UNIT-VECTOR-NORM}(\mathbf{f} - \mathbf{m}_i)$ ;
5    $\mathbf{x}_i = \|(\tilde{\mathbf{f}}_i - \boldsymbol{\mu}_i)\|^2$ ;
6    $y = y + \frac{p_i(\mathbf{x}_i)}{K}$ 
7 return  $y$  # an estimate of  $p(\alpha|\mathbf{f})$ .

```

	Average AUROC for each data-set				
	Fashion -MNIST	STL-10	Internet STL-10	MIT- Places	ASSIRA
OC-SVM [9]	0.892 (I)	0.799 (R)	0.557 (R)	0.765 (R)	0.824 (R)
SO-Ours	0.911 (I)	0.958 (R)	0.948 (R)	0.910 (R)	0.964 (R)
SS-Ours	0.953 (I)	0.987 (R)	0.975 (R)	0.983 (R)	0.994 (R)
OC-NN [8]	0.851 (I)	0.949 (R)	0.932 (R)	0.895 (R)	0.932 (R)
Deep A.Det. [19]	0.935 (I)	0.730 (I)	0.717 (I)	0.722 (I)	0.888 (I)
DSEBM [46]	0.884 (I)	0.571 (I)	0.560 (I)	0.613 (I)	0.516 (I)
DAGMM [48]	0.518 (I)	0.554 (I)	0.517 (I)	0.530 (I)	0.485 (I)
AD-GAN [11]	0.884 (I)	0.602 (I)	0.555 (I)	0.499 (I)	0.534 (I)

Table 1: AUROC score of various one-class learners. Inputs are indicated with (I) for raw images and (R) for ResNet features. Shells-Stacked (SS) results are noticeably good, indirectly validating the *hierarchical-model* used in its design.

Fundamentally, the *hierarchical-model* is a theory of data generation. The usefulness of such theories depend on their predictive and explanatory power.



A Precision-Recall curve comparing three models: SS (blue line with circles), SO (orange line with circles), and OC-SVM (green line with circles). The x-axis is Precision (0.0 to 1.0) and the y-axis is Recall (0.0 to 1.0). The OC-SVM curve shows high recall at low precision, while the SS and SO curves show high recall across most precision values, with SS slightly outperforming SO at higher precision values.

Precision	SS Recall	SO Recall	OC-SVM Recall
0.0	0.0	0.0	0.0
0.1	1.0	1.0	0.9
0.2	1.0	1.0	0.9
0.4	0.95	0.9	0.9
0.6	0.85	0.75	0.85
0.8	0.65	0.55	0.65
1.0	0.0	0.0	0.0

Figure 3: Recall vs Precision from integrating multiple one-class learners for multiclass classification. This can be achieved with shell-learners like SO and SS. With traditional one-class learners like OC-SVM, each learner has a unique range of values, creating the vertical zig-zag line seen above.

One-class SVM with traditional normalization creates very poor results. This is predicted in Sec. 4.2 and demonstrated in Sec. 8.2 of the supplementary; C) Shell-Learning should work, as demonstrated in Sec. 5.2.

Explanatory power is demonstrated by three examples: I) Supplementary Sec. 7.2 shows high dimensional Euclidean distance remains meaningful. This differs from our current paradigm in which they are “cursed” [2] and provides a mathematical model that accommodates the very high dimensional, yet very effective deep-learned features [3, 21, 37]; II) In the *hierarchical-model*, small differences in distribution parameters suffice to ensure separability of their instances. If deep-learners are exploiting such properties, they could be both robust in practice but easily fooled by deliberate perturbations [30]. This creates a plausible explanation for a long-standing puzzle; III) Sec. 4.2 explains how and why data should be normalized, a concept systematically exploited by our SS algorithm in Sec. 4.4. Previously, normalization’s importance was well documented [4] but there was little justification for its effectiveness.

SO and SS refer to Sec. 4.4’s Shell-One and Shell-Stacked algorithms. By strict definitions, SO and SS are not one-class learners as feature choice and normalization embed assumptions on external distributions. In particular, SS treats the means of other training data as external knowledge for estimating parent distribution means. However, given the omnipresence of the internet, such assumptions are not restrictive. While comparing algorithm scores does not represent fair competition, it creates a baseline for assessing *hierarchical-model*’s relevance in the real-world.

Data-sets are described by, name; [citation]; (number of training images per class). They are: Fashion-MNIST [44]

	airplane (ship)	bird (cat)	car (truck)	cat (dog)	deer (horse)	dog (cat)	horse (dog)	monkey (dog)	ship (truck)	truck (car)	Average
SO-Ours	0.886	0.970	0.842	0.713	0.884	0.746	0.701	0.929	0.897	0.619	0.819
SS-Ours	0.972	0.994	0.933	0.826	0.954	0.927	0.914	0.969	0.942	0.784	0.922

	abbey (alley)	airport terminal (amusement park)	alley (airport terminal)	amusement park (airport terminal)	aquarium (amusement park)	Average
SO-Ours	0.829	0.909	0.895	0.703	0.824	0.832
SS-Ours	0.965	0.959	0.981	0.938	0.954	0.959

Table 2: AUROC on the most difficult class pairs of Internet STL-10 and MIT-Places. Shells-Stacked’s (SS) gain over Shells-One (SO) is much more noticeable.

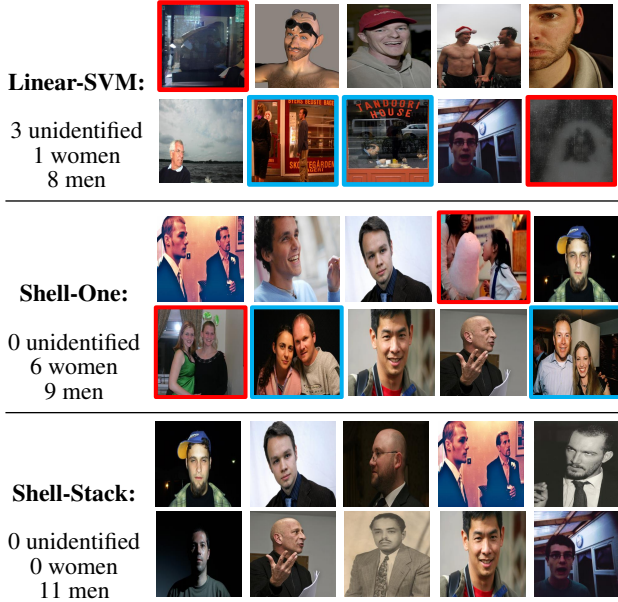


Figure 4: Learning to detect “man” in Flickr11k [24]. Training images are crawled from the web with semantic search words. Top 10 returns of each algorithm are shown. Errors are boxed in red, partial errors in blue. Discriminative learners like linear-SVM perform poorly on such open-set tasks. Generative shell-learners are better as they estimate the probability of a class given the image.

(10,000); STL-10 [10] (500); Internet STL-10 [10] (variable); MIT-Places first 5 classes [47] (1000); ASSIRA [16] (1000). STL-10 and ASSIRA represent standard benchmarks for one-class learning. Fashion-MNIST and MIT-Places contain less typical concepts that features are not pre-trained on. Finally, Internet STL-10 tests algorithm’s noise handling by having a training set that consist **solely** of Internet crawled images and a testing set of STL-10 images.

Baseline algorithms are one-class SVM [9] and state-of-art deep-learned alternatives [46, 19, 48, 11, 8]. The deep-learners typically couple an auto-encoder to some cost function, creating an end-to-end learning framework that can modify all stages for better performance. In some architectures, replacing end-to-end learning with ResNet features improves performance. For such cases, ResNet features are

used as input. Results are tabulated in Table 1.

SS and SO provide simple learning frameworks that are competitive with or better than far more complicated alternatives. SS’s performance is so good that when trained solely with internet data in Internet STL, its performance is still better than any learner trained on un-corrupted STL-10 data. SS’s performance gains are especially pronounced on challenging data. This is illustrated in Table 2, which shows performance on the most ambiguous class pairs in Internet STL-10 and MIT-Places. We believe these results indirectly validate the *hierarchical-model* used to design SS and SO.

5.3. Shell Learners as Classifiers

Multiple independently trained shell-learners can be used to perform multiclass classification by assigning each instance to the highest scoring learner. On this task, SS’s average precision over all data-sets is 0.862. This is only slightly below discriminative classifiers like linear-SVM at 0.899 and much higher than radial-basis-kernel SVM at 0.437, whose density based formulation may be inappropriate for high dimensions where density vanishes.

These are remarkable results that, to our knowledge, have never been demonstrated by one-class learning formulations [22]. Figure 3 shows utilizing one-class SVM on the same task creates a vertical zig-zag precision-recall line, corresponding to each learner creating its own unique range of scores. The results are still more remarkable when we recall SS is a generative formulation, which trades some discriminative performance [29] for open-set capability demonstrated in Fig. 4.

6. Conclusion

This paper suggests many data generation processes can be explained by a *hierarchical-model*. This makes it possible to mathematically formulate open-set problems that often seem impossible to analyze rigorously. We demonstrate this with a one-class learning formulation that adds new classes to a model without needing retraining. This creates the exciting prospect of life-long learners that can expand their understanding indefinitely [22].

References

- [1] https://en.wikipedia.org/wiki/Curse_of_dimensionality. Accessed: 2019-11-15. 1
- [2] Charu C Aggarwal, Alexander Hinneburg, and Daniel A Keim. On the surprising behavior of distance metrics in high dimensional space. In *International conference on database theory*, pages 420–434. Springer, 2001. 1, 2, 3, 7
- [3] Relja Arandjelovic, Petr Gronat, Akihiko Torii, Tomas Pajdla, and Josef Sivic. Netvlad: Cnn architecture for weakly supervised place recognition. In *Proceedings of IEEE Conference on Computer Vision and Pattern Recognition (CVPR)*, pages 5297–5307, 2016. 2, 7
- [4] Relja Arandjelovic and Andrew Zisserman. All about vlad. In *Proceedings of IEEE Conference on Computer Vision and Pattern Recognition (CVPR)*, pages 1578–1585, 2013. 7
- [5] Abhijit Bendale and Terrance E Boult. Towards open set deep networks. In *Proceedings of IEEE Conference on Computer Vision and Pattern Recognition (CVPR)*, pages 1563–1572, 2016. 1
- [6] David M Blei, Andrew Y Ng, and Michael I Jordan. Latent dirichlet allocation. In *Proceedings of Advances in Neural Information Processing Systems (NIPS)*, pages 601–608, 2002. 2
- [7] George EP Box and George C Tiao. Multiparameter problems from a bayesian point of view. *The Annals of Mathematical Statistics*, 36(5):1468–1482, 1965. 2
- [8] Raghavendra Chalapathy, Aditya Krishna Menon, and Sanjay Chawla. Anomaly detection using one-class neural networks. *arXiv preprint arXiv:1802.06360*, 2018. 7, 8
- [9] Yunqiang Chen, Xiang Sean Zhou, and Thomas S Huang. One-class svm for learning in image retrieval. In *Proceedings of IEEE International Conference on Image Processing (ICIP)*, pages 34–37. Citeseer, 2001. 1, 2, 5, 7, 8, 13, 15, 16
- [10] Adam Coates, Andrew Ng, and Honglak Lee. An analysis of single-layer networks in unsupervised feature learning. In *Proceedings of the fourteenth international conference on artificial intelligence and statistics*, pages 215–223, 2011. 8, 13, 14, 15
- [11] Lucas Deecke, Robert Vandermeulen, Lukas Ruff, Stephan Mandt, and Marius Kloft. Anomaly detection with generative adversarial networks. <https://openreview.net/forum?id=S1EfyIZ0Z>, 2018. 7, 8
- [12] Frank Dellaert. The expectation maximization algorithm. Technical report, Georgia Institute of Technology, 2002. 2
- [13] Arthur P Dempster, Nan M Laird, and Donald B Rubin. Maximum likelihood from incomplete data via the em algorithm. *Journal of the Royal Statistical Society: Series B (Methodological)*, 39(1):1–22, 1977. 2
- [14] Pedro M Domingos. A few useful things to know about machine learning. *Commun. acm*, 55(10):78–87, 2012. 1
- [15] Alexey Dosovitskiy and Thomas Brox. Generating images with perceptual similarity metrics based on deep networks. *Proceedings of Advances in Neural Information Processing Systems (NIPS)*, pages 658–666, 2016. 2
- [16] Jeremy Elson, John (JD) Douceur, Jon Howell, and Jared Saul. Asirra: A captcha that exploits interest-aligned manual image categorization. In *Proceedings of 14th ACM Conference on Computer and Communications Security (CCS)*. Association for Computing Machinery, Inc., October 2007. 8, 14, 15
- [17] Nir Friedman, Dan Geiger, and Moises Goldszmidt. Bayesian network classifiers. *Machine learning*, 29(2-3):131–163, 1997. 2
- [18] Andrew Gelman, John B Carlin, Hal S Stern, David B Dunson, Aki Vehtari, and Donald B Rubin. *Bayesian data analysis*. Chapman and Hall/CRC, 2013. 2
- [19] Izhak Golan and Ran El-Yaniv. Deep anomaly detection using geometric transformations. In *Proceedings of Advances in Neural Information Processing Systems (NIPS)*, pages 9758–9769, 2018. 7, 8, 15
- [20] Ian Goodfellow, Jean Pouget-Abadie, Mehdi Mirza, Bing Xu, David Warde-Farley, Sherjil Ozair, Aaron Courville, and Yoshua Bengio. Generative adversarial nets. In *Proceedings of Advances in Neural Information Processing Systems (NIPS)*, pages 2672–2680, 2014. 2
- [21] Kaiming He, Xiangyu Zhang, Shaoqing Ren, and Jian Sun. Deep residual learning for image recognition. In *Proceedings of IEEE Conference on Computer Vision and Pattern Recognition (CVPR)*, pages 770–778, 2016. 2, 6, 7, 13, 16
- [22] Navid Kardan and Kenneth O Stanley. Fitted learning: Models with awareness of their limits. *arXiv preprint arXiv:1609.02226*, 2016. 1, 2, 8
- [23] Diederik P Kingma and Max Welling. Auto-encoding variational bayes. In *Proceedings of International Conference on Learning Representations (ICLR)*, 2014. 2
- [24] Yin-Hsi Kuo, Hsuan-Tien Lin, Wen-Huang Cheng, Yi-Hsuan Yang, and Winston H Hsu. Unsupervised auxiliary visual words discovery for large-scale image object retrieval. In *Proceedings of IEEE Conference on Computer Vision and Pattern Recognition (CVPR)*, pages 905–912, 2011. 8
- [25] Wen-Yan Lin, Siying Liu, Jian-Huang Lai, and Yasuyuki Matsushita. Dimensionality’s blessing: Clustering images by underlying distribution. In *Proceedings of IEEE Conference on Computer Vision and Pattern Recognition (CVPR)*, pages 5784–5793, 2018. 1, 2
- [26] Laurens van der Maaten and Geoffrey Hinton. Visualizing data using t-sne. *Journal of machine learning research*, 9(Nov):2579–2605, 2008. 2
- [27] Leland McInnes, John Healy, and James Melville. Umap: Uniform manifold approximation and projection for dimension reduction. *arXiv preprint arXiv:1802.03426*, 2018. 2
- [28] Todd K Moon. The expectation-maximization algorithm. *IEEE Signal processing magazine*, 13(6):47–60, 1996. 2
- [29] Andrew Y Ng and Michael I Jordan. On discriminative vs. generative classifiers: A comparison of logistic regression and naive bayes. In *Proceedings of Advances in Neural Information Processing Systems (NIPS)*, pages 841–848, 2002. 8

- [30] Anh Nguyen, Jason Yosinski, and Jeff Clune. Deep neural networks are easily fooled: High confidence predictions for unrecognizable images. In *Proceedings of IEEE Conference on Computer Vision and Pattern Recognition (CVPR)*, pages 427–436, 2015. 7
- [31] Poojan Oza and Vishal M Patel. C2ae: Class conditioned auto-encoder for open-set recognition. In *Proceedings of IEEE Conference on Computer Vision and Pattern Recognition (CVPR)*, 2019. 1
- [32] German I Parisi, Ronald Kemker, Jose L Part, Christopher Kanan, and Stefan Wermter. Continual lifelong learning with neural networks: A review. *Neural Networks*, 2019. 2
- [33] Karl Pearson. Liii. on lines and planes of closest fit to systems of points in space. *The London, Edinburgh, and Dublin Philosophical Magazine and Journal of Science*, 2(11):559–572, 1901. 2
- [34] Miloš Radovanović, Alexandros Nanopoulos, and Mirjana Ivanović. Reverse nearest neighbors in unsupervised distance-based outlier detection. *IEEE transactions on knowledge and data engineering*, 27(5):1369–1382, 2015. 1
- [35] Bryan C Russell, William T Freeman, Alexei A Efros, Josef Sivic, and Andrew Zisserman. Using multiple segmentations to discover objects and their extent in image collections. In *Proceedings of IEEE Conference on Computer Vision and Pattern Recognition (CVPR)*, volume 2, pages 1605–1614, 2006. 2
- [36] David W Scott. The curse of dimensionality and dimension reduction. *Multivariate Density Estimation: Theory, Practice, and Visualization*, pages 195–217, 2008. 2
- [37] Karen Simonyan and Andrew Zisserman. Very deep convolutional networks for large-scale image recognition. *arXiv preprint arXiv:1409.1556*, 2014. 2, 7
- [38] George Gaylord Simpson. Principles of animal taxonomy. 1961. 1
- [39] Josef Sivic, Bryan C Russell, Andrew Zisserman, William T Freeman, and Alexei A Efros. Unsupervised discovery of visual object class hierarchies. In *Proceedings of IEEE Conference on Computer Vision and Pattern Recognition (CVPR)*, pages 1–8, 2008. 2
- [40] Tod F Stuessy. *Plant taxonomy: the systematic evaluation of comparative data*. Columbia University Press, 2009. 1
- [41] Gabor J Szekely and Maria L Rizzo. Hierarchical clustering via joint between-within distances: Extending ward’s minimum variance method. *Journal of classification*, 22(2):151–183, 2005. 1
- [42] Nenad Tomasev, Milos Radovanovic, Dunja Mladenic, and Mirjana Ivanovic. The role of hubness in clustering high-dimensional data. *IEEE Transactions on Knowledge and Data Engineering*, 26(3):739–751, 2014. 1
- [43] Peter F Windley. Trees, forests and rearranging. *The Computer Journal*, 3(2):84–88, 1960. 1
- [44] Han Xiao, Kashif Rasul, and Roland Vollgraf. Fashion-mnist: a novel image dataset for benchmarking machine learning algorithms. *arXiv preprint arXiv:1708.07747*, 2017. 7
- [45] Ryota Yoshihashi, Wen Shao, Rei Kawakami, Shaodi You, Makoto Iida, and Takeshi Naemura. Classification-reconstruction learning for open-set recognition. In *Proceedings of IEEE Conference on Computer Vision and Pattern Recognition (CVPR)*, pages 4016–4025, 2019. 1
- [46] Shuangfei Zhai, Yu Cheng, Weining Lu, and Zhongfei Zhang. Deep structured energy based models for anomaly detection. *arXiv preprint arXiv:1605.07717*, 2016. 7, 8
- [47] Bolei Zhou, Agata Lapedriza, Jianxiong Xiao, Antonio Torralba, and Aude Oliva. Learning deep features for scene recognition using places database. In *Proceedings of Advances in Neural Information Processing Systems (NIPS)*, pages 487–495, 2014. 8, 14, 15
- [48] Bo Zong, Qi Song, Martin Renqiang Min, Wei Cheng, Cristian Lumezanu, Daeki Cho, and Haifeng Chen. Deep autoencoding gaussian mixture model for unsupervised anomaly detection. In *Proceedings of International Conference on Learning Representations (ICLR)*, 2018. 7, 8

7. Supplementary Material (Theoretical)

7.1. Proof for Re-Normalization Corollary

Before proving Corollary 2, we need to introduce a Lemma:

Lemma 1. *A distribution's mean, one of it's sub-distribution's mean and an arbitrarily point $\mathbf{c} \in \mathbb{R}^k$ almost surely form a right-angled triangle,*

$$d^2(\mathbf{M}_{\theta^n \Theta^j} - \mathbf{c}) \stackrel{a.s.}{=} d^2(\mu_{\theta^n} - \mathbf{c}) + d^2(\mathbf{M}_{\theta^n \Theta^j} - \mu_{\theta^n}) \quad (24)$$

Proof. From Eq. (2) and Theorem 2,

$$\begin{aligned} & d^2(\mathbf{A}_{\theta^n \Theta^j} - \mathbf{c}) \\ & \stackrel{a.s.}{=} V_{\theta^n \Theta^j} + d^2(\mathbf{M}_{\theta^n \Theta^j} - \mathbf{c}) \\ & \stackrel{a.s.}{=} v_{\theta^{[n]}} - d^2(\mathbf{M}_{\theta^n \Theta^j} - \mu_{\theta^{[n]}}) + d^2(\mathbf{M}_{\theta^n \Theta^j} - \mathbf{c}) \end{aligned} \quad (25)$$

$$d^2(\mathbf{A}_{\theta^n \Theta^j} - \mathbf{c}) \stackrel{a.s.}{=} d^2(\mathbf{A}_{\theta^n} - \mathbf{c}) \stackrel{a.s.}{=} v_{\theta^{[n]}} + d^2(\mu_{\theta^{[n]}} - \mathbf{c}) \quad (26)$$

Combining Eq. (25), Eq. (26), yields

$$d^2(\mathbf{M}_{\theta^n \Theta^j} - \mathbf{c}) \stackrel{a.s.}{=} d(\mu_{\theta^n} - \mathbf{c}) + d^2(\mathbf{M}_{\theta^n \Theta^j} - \mu_{\theta^n})$$

□

Using Lemma 1, the proof for the Re-Normalization Corollary 2 is:

Proof. If l is an ancestor of both m, n , it can be considered a distribution-of-everything encompassing both sub-distributions. Thus, re-normalizing with mean μ_{θ^l} only involves a translation and division by a scalar common to both m and n . Thus, from Eq. (22), $\widetilde{g}_{mn} = \frac{2(v_{\theta^m} - v_{\theta^n})}{v_{\theta^l}}$, proving the first case of Eq. (23).

For the case $l \leq m$, with θ^m representing a parent of θ^l . After re-normalization with μ_{θ^l} , almost-surely:

$$\begin{aligned} \mu_{\widetilde{\theta}^l} &= \mathbf{0}; \\ v_{\widetilde{\theta}^n} + d^2(\mu_{\widetilde{\theta}^n}) &= 1; \quad \text{because } d^2(\widetilde{\mathbf{A}}_{\widetilde{\theta}^n} - \mathbf{0}) \stackrel{a.s.}{=} 1 \\ v_{\widetilde{\theta}^m} + d^2(\mu_{\widetilde{\theta}^m}) &= 1; \quad \text{because } d^2(\widetilde{\mathbf{A}}_{\widetilde{\theta}^m} - \mathbf{0}) \stackrel{a.s.}{=} 1 \end{aligned} \quad (27)$$

Replacing \mathbf{c} in Lemma 1, with $\mu_{\widetilde{\theta}^m}$,

$$d^2(\mathbf{M}_{\widetilde{\theta}^l \Theta^j} - \mu_{\widetilde{\theta}^m}) \stackrel{a.s.}{=} d^2(\mu_{\widetilde{\theta}^m} - \mu_{\widetilde{\theta}^l}) + d^2(\mathbf{M}_{\widetilde{\theta}^l \Theta^j} - \mu_{\widetilde{\theta}^l}). \quad (28)$$

As $\mu_{\widetilde{\theta}^n}$ is an instance of $\mathbf{M}_{\widetilde{\theta}^l \Theta^j}$, Eq. (27) and Eq. (28), almost-surely result in

$$\begin{aligned} d^2(\mu_{\widetilde{\theta}^n} - \mu_{\widetilde{\theta}^m}) &= d^2(\mu_{\widetilde{\theta}^m} - \mu_{\widetilde{\theta}^l}) + d^2(\mu_{\widetilde{\theta}^n} - \mu_{\widetilde{\theta}^l}) \\ &= d^2(\mu_{\widetilde{\theta}^m}) + d^2(\mu_{\widetilde{\theta}^n}) \end{aligned} \quad (29)$$

Combining Eq. (2), Eq. (27), Eq. (29), almost-surely

$$\begin{aligned} d^2(\widetilde{\mathbf{A}}_{\widetilde{\theta}^m \Theta^i} - \mu_{\widetilde{\theta}^n}) &\stackrel{a.s.}{=} v_{\widetilde{\theta}^m} + d^2(\mu_{\widetilde{\theta}^m} - \mu_{\widetilde{\theta}^n}) \\ &= v_{\widetilde{\theta}^m} + d^2(\mu_{\widetilde{\theta}^m}) + d(\mu_{\widetilde{\theta}^n}) \\ &= 2 - v_{\widetilde{\theta}^n} \end{aligned} \quad (30)$$

This proves the last case in Eq. (23),

$$\widetilde{g}_{mn} = 2(1 - v_{\widetilde{\theta}^n}) = \frac{2(v_{\theta^l} - v_{\theta^n})}{v_{\theta^l}} \quad (31)$$

□

7.2. Euclidean Distance in High Dimensions

In the *hierarchical-model*, the Euclidean distance between two high dimension instances is almost-surely a reflection of how recently they shared a common ancestor. This is summarized in the Euclidean distance corollary below:

Corollary 3. (*Euclidean distance*) *In a non-trivial hierarchical-model, ranking data points by euclidean distance from \mathbf{a} , is almost surely, ranking based on how recently they shared an ancestor with \mathbf{a} .*

Proof. Let \mathbf{a} be an instance of A_{θ^m} , where

$$\theta^m = \theta^{[0]} \theta^{[1]} \theta^{[2]} \dots \theta^{[m]},$$

is an instantiation of a non-trivial hierarchical process. The average variance corresponding to the parameters $\theta^{[i]}$ is $v_{\theta^{[i]}}$. From corollary 1, almost surely,

$$v_{\theta^{[0]}} > v_{\theta^{[1]}} > v_{\theta^{[2]}} > \dots > v_{\theta^{[m]}}.$$

For any data-point \mathbf{p} in the *hierarchical-model*, Theorem 1 implies, almost-surely, $d^2(\mathbf{a} - \mathbf{p}) = 2v_{\theta^{[i]}}$, where i is the index of their most recent common ancestor. Thus, ranking based euclidean distance from \mathbf{a} ; is almost-surely, ranking based on average variance of the most recent ancestor; is almost-surely, ranking based on how recently the points shared an ancestor. □

7.3. Predicted Distance Histograms

This section analyzes distances with deep-learned features to see if they follow the patterns predicted by the *hierarchical-model*. Results for real and simulated data are displayed in Fig. 5.

A) Statistical maximum pair-wise distance is $\sqrt{2}$: Recall that for unit-vector-normalized data,

$$d^2(\mathbf{A} - \mathbf{0}) \stackrel{a.s.}{=} v_{\mathbf{A}} + d^2(\mu_{\mathbf{A}} - \mathbf{0}) = 1.$$

Thus, $v_{\mathbf{A}} \leq 1$ From Fig. 2 and Corollary 3, the distance between any two instances is almost-surely less than or equal to $\sqrt{2v_{\mathbf{A}}}$ which is in turn less than or equal to $\sqrt{2}$. This

creates a statistical maximum pairwise distance is $\sqrt{2}$ that is much less than the geometric maximum of 2.

B) Distance to random unit-vector almost-surely constant:

From Eq. (2)

$$d^2(\mathbf{A}_{\Theta^i} - \mathbf{c}) \stackrel{a.s.}{=} v_{\mathbf{A}} + d(\boldsymbol{\mu}_{\mathbf{A}} - \mathbf{c}) = \text{constant}. \quad (32)$$

This equation has often been mis-interpreted as a “curse”. While this is true, a different pattern emerges when considering pairwise distances;

C) Log pairwise histogram shows a variety of distances: From theorem 1 and Fig. 2, not all pairwise distances are constants. While many pairwise distances converge to $\sqrt{2}v_{\mathbf{A}}$, the log histogram displays a variety of distances.

8. Supplementary Material (Empirical)

8.1. Errors

Figure 6 shows distances of instances from a shell’s center. Labels are color coded. The shell is trained with instances of the red class. Observe that in practice, distances do not lie and a perfect constant but form a cloud. Despite this, points of the red class are separable from the rest. Separability can be increased through re-normalization in Sec. 4.2.

8.2. Normalization in One-Class Learning

To date, there has been no clear guide on how to perform normalization in one-class learning. Table 3 shows traditional normalization which involves centering data and converting it to unit-vectors causes extremely poor results. This was predicted in 4.2. As a result one-class learning papers perform no normalization. Table 3.

8.3. Shell-Learning vs One-Class SVM

Given properly normalized data, shell-learning (SO) is similar to one-class SVM. However, there is a significant difference in more difficult conditions. Figure 7 shows the effect of shifting the mean used for normalization towards a target class, the degenerate case given in Eq. (23). Observe that while shell-learning’s performance decreases, it remains much more stable than one-class SVM.

8.4. Magic of Deep Learning Features

Applying one-class SVM on deep-learned features creates magically good results. Much of this result is because deep-learned features use a coordinate frame in which zero corresponds to the mean of the distribution-of-everything. Shifting the coordinate frame causes a marked deterioration in the results as shown in Fig. 8.

8.5. Effect of Shells-Stacked (SS)

Figure 9 plots the one-class detection AUROC score on STL-10 dataset, with increasingly stacked shells. This shows the effectiveness of re-normalization in incorporating external knowledge into a one-class learning framework.

8.6. Mean-Variance Constraint Predicted by Hierarchical-Model

Sec. 3.1 shows that the parent and child distributions generated by a *hierarchical process* in the *hierarchical-model* must adhere to Theorem 2. Results in Table 4 shows that this relationship in real-world data follows the mean-variance constraint predicted by our *hierarchical-model*. Statistics for various fine-grained types of dogs and cats are collected from ImageNet data under Domestic Animal-(Domestic Dog, Domestic Cat) hierarchical synsets. Animals and transports data are from STL-10 dataset. Images are converted into ResNet features using pretrained ResNet50 and unit-normalized.

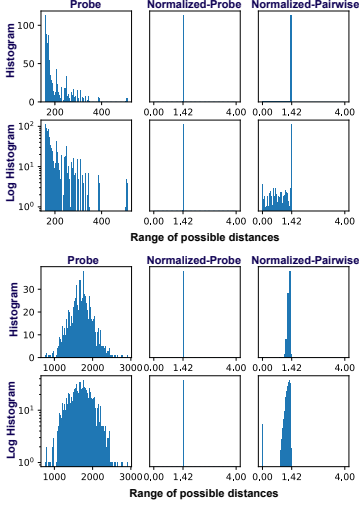


Figure 5: **Probe** is the histogram of the distance of all data-set instances to a single, unit vector probe. Data derived from a hierarchical-process, will have a histogram sharply peaked at some point. This is clearly not the case for both simulated and real-data. **Normalized-Probe** involves unit-vector-normalization of all data before computing their distance to the probe. Data derived from a hierarchical-process perturbed by some scaling functions will have histograms which peak sharply at $\sqrt{2} = 1.42$. This happens for both simulated and real-data. **Normalized-Pairwise** is the histogram of pair-wise distance between data-set points. Data derived from complex hierarchical-processes, have histograms that peak sharply at 1.42 but the log histogram should show some instances that are less than 1.42. 1.42 is the statistical maximum distance which almost no distance should exceed. **Summary:** A hierarchical-process with scalar perturbations is an eerily accurate model of real-world data. This is reflected in histograms which exhibit the surprising characteristics predicted by the hierarchical-processes and in our ability to create simulations that mimic these characteristics.

	STL-10 [10] (ResNet Features [21])										
	airplane	bird	car	cat	deer	dog	horse	monkey	ship	truck	Ave.
OC-SVM(no-normalization)	0.854	0.748	0.949	0.689	0.857	0.553	0.792	0.709	0.929	0.905	0.799
OC-SVM(traditional-normalization)	0.550	0.458	0.670	0.468	0.492	0.351	0.565	0.471	0.722	0.472	0.522

Table 3: AUROC score of OC-SVM [9] on STL-10. As predicted in Sec. 4.2, traditional normalization makes one-class learning very much worse. As such normalization is seldom performed.

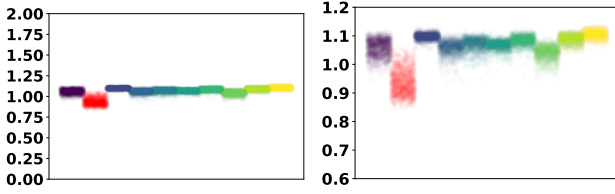


Figure 6: Distances to shell center for the “bird” class in STL-10 [10]. Colors represent different classes of STL-10 dataset. Red color represents the ‘bird’ class to which the shell is fitted.

Variances and means are calculated based on unit-normalized ResNet features. Low error ratio indicates the mean-variance relationship of parent and child distributions in real-world data is consistent with Theorem 2.

8.7. Detailed Precision Scores for Each Class in Different Datasets

We provide detailed numbers of multi-class recognition precision scores for each class in all the datasets we tested in Table 5.

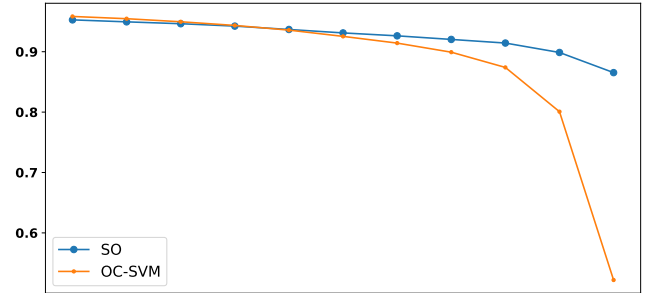


Figure 7: Average AUROC score on STL-10 dataset, with increasingly poor normalization. Observe that shell-learning (SO) is much more robust than traditional one-class SVM [9] to poor normalization.

8.8. Detailed AUROC Scores for Each Class in Different Datasets

We provide detailed numbers of one-class detection AUROC scores for each class in all the datasets we tested in Table 6.

8.9. Clustering

The *shell based learning* can also be applied to the problem of unsupervised clustering. The result is illustrated in Fig. 10, where we conduct unsupervised cluster-

Parent Distribution	Average Variance of Parent Distribution	Mean Average Variance of Sub-Distribution + NSD of Mean Vectors for all Sub-Distributions	Error Ratio
\mathbf{A}_{θ^n}	$v_{\theta^{[n]}}$	$V_{\theta^n \Theta^j} + d^2(\mathbf{M}_{\theta^n \Theta^j} - \mu_{\theta^{[n]}})$	%
Domestic Dog	0.000308	0.000309	0.039%
Poodle Dog	0.000260	0.000264	1.794%
Spitz	0.000253	0.000259	2.363%
Shepherd Dog	0.000300	0.000300	0.289%
Sled Dog	0.000235	0.000245	4.113%
Watch Dog	0.000298	0.000303	1.857%
Sennenhunde	0.000229	0.000229	0.041%
Working Dog	0.000306	0.000306	0.125%
Domestic Cat	0.000269	0.000268	0.119%
Animals	0.000337	0.000337	0.000%
Transports	0.000336	0.000336	0.000%

Table 4: Average variance of parent distribution, and predicted average variance of parent distribution using Theorem 2, and the respective error ratio in percentage.

A) Fashion-MNIST (Raw Image)											
	t-shirt	trouser	pullover	dress	coat	sandal	shirt	sneaker	bag	boot	Ave.
SS-Ours	0.802	0.996	0.565	0.718	0.508	0.801	0.292	0.905	0.924	0.913	0.742
SVM(Linear)	0.812	0.968	0.713	0.799	0.691	0.951	0.669	0.901	0.912	0.920	0.834
SVM(RBF Kernel)	0.000	0.295	0.081	0.000	0.000	0.000	0.197	0.468	0.000	0.721	0.176
B) STL-10 [10] (ResNet-50 Features)											
	airplane	bird	car	cat	deer	dog	horse	monkey	ship	truck	Ave.
SS-Ours	0.922	0.969	0.961	0.779	0.891	0.729	0.861	0.938	0.894	0.803	0.875
SVM(Linear)	0.935	0.954	0.951	0.885	0.895	0.862	0.903	0.909	0.909	0.888	0.909
SVM(RBF Kernel)	0.958	0.948	0.927	0.908	0.794	0.659	0.950	0.909	0.805	0.813	0.867
C) Internet STL-10 (ResNet-50 Features)											
	airplane	bird	car	cat	deer	dog	horse	monkey	ship	truck	Ave.
SS-Ours	0.646	0.626	0.941	0.910	0.706	0.572	0.936	0.964	0.857	0.870	0.803
SVM(Linear)	0.780	0.816	0.873	0.877	0.687	0.722	0.934	0.936	0.798	0.850	0.827
SVM(RBF Kernel)	0.000	0.100	0.000	0.000	0.000	0.000	0.000	0.000	0.000	0.000	0.010
D) MIT-Places [47]						E) Assira [16]					
	abbey	airport terminal	alley	amusement park	aquarium	Ave.	cat	dog	Ave.		
SS-Ours	0.955	0.896	0.919	0.772	0.955	0.899	0.995	0.971	0.983		
SVM(Linear)	0.936	0.941	0.946	0.911	0.962	0.939	0.989	0.990	0.990		
SVM(RBF Kernel)	0.945	0.905	0.915	0.723	0.924	0.882	0.000	0.500	0.250		

Table 5: Precision score of various multi-class classifiers. Integration of multiple SS as a multi-class classifier achieves recognition precision only slightly below Linear SVM in most cases.

ing on a mixed dataset consisting of images from three classes, namely cat, dog and panda. Images are converted to 2048-dimensional feature vectors using pretrained ResNet50 model followed by unit-normalization operation, after which our shell based learning model searches for three different distinctive shells of the three classes. We plot the distances

of each data point to each distinctive shell. Color of the points represents their ground-truth class label. The shells returned by our model are occupied almost solely by feature points of its corresponding label, and the points are separated nicely according to their distances to the distinctive shells. This preliminary experiment reveals the great potential of

A) Fashion-MNIST (Raw Image)											
	t-shirt	trouser	pullover	dress	coat	sandal	shirt	sneaker	bag	boot	Ave.
OC-SVM [9]	0.884	0.972	0.857	0.900	0.876	0.868	0.787	0.982	0.816	0.976	0.892
SO-Ours	0.911	0.975	0.881	0.912	0.904	0.921	0.772	0.986	0.856	0.990	0.911
SS-Ours	0.954	0.988	0.921	0.967	0.931	0.975	0.830	0.989	0.981	0.991	0.953
OC-NN	0.818	0.963	0.739	0.917	0.916	0.932	0.678	0.948	0.614	0.982	0.851
Deep A.Det [19]	0.918	0.981	0.916	0.879	0.898	0.934	0.827	0.991	0.987	0.994	0.932
DSEBM	0.916	0.718	0.883	0.873	0.852	0.871	0.734	0.981	0.860	0.971	0.884
DAGMM	0.421	0.551	0.504	0.571	0.269	0.705	0.483	0.835	0.499	0.340	0.518
AD-GAN	0.899	0.819	0.876	0.912	0.865	0.896	0.743	0.972	0.890	0.971	0.884

B) STL-10 [10] (ResNet-50 Features)											
	airplane	bird	car	cat	deer	dog	horse	monkey	ship	truck	Ave.
OC-SVM	0.854	0.748	0.949	0.689	0.857	0.553	0.792	0.709	0.929	0.905	0.799
SO-Ours	0.974	0.965	0.985	0.894	0.962	0.928	0.960	0.962	0.983	0.969	0.958
SS-Ours	0.993	0.994	0.993	0.976	0.981	0.978	0.984	0.992	0.993	0.987	0.987
OC-NN	0.973	0.962	0.969	0.881	0.955	0.894	0.952	0.966	0.972	0.971	0.949
Deep A.Det.	0.575	0.544	0.801	0.632	0.819	0.725	0.841	0.858	0.797	0.706	0.730
DSEBM	0.677	0.590	0.425	0.630	0.735	0.569	0.534	0.639	0.607	0.308	0.571
DAGMM	0.729	0.503	0.613	0.596	0.647	0.479	0.591	0.519	0.235	0.627	0.554
AD-GAN	0.751	0.570	0.480	0.600	0.772	0.623	0.508	0.582	0.671	0.465	0.602

C) Internet STL-10 (ResNet-50 Features)											
	airplane	bird	car	cat	deer	dog	horse	monkey	ship	truck	Ave.
OC-SVM	0.733	0.403	0.895	0.442	0.464	0.246	0.419	0.275	0.860	0.835	0.557
SO-Ours	0.959	0.971	0.977	0.876	0.965	0.922	0.946	0.960	0.980	0.926	0.948
SS-Ours	0.983	0.990	0.989	0.923	0.982	0.973	0.976	0.987	0.990	0.955	0.975
OC-NN	0.939	0.955	0.967	0.851	0.949	0.891	0.938	0.941	0.968	0.921	0.932
Deep A.Det.	0.528	0.616	0.834	0.697	0.774	0.695	0.844	0.803	0.695	0.686	0.717
DSEBM	0.743	0.582	0.272	0.582	0.750	0.571	0.548	0.633	0.633	0.289	0.560
DAGMM	0.607	0.500	0.486	0.481	0.564	0.530	0.485	0.619	0.408	0.489	0.517
AD-GAN	0.743	0.533	0.406	0.550	0.734	0.558	0.501	0.604	0.618	0.306	0.555

D) MIT-Places [47]							E) Assira [16]		
	abbey	airport terminal	alley	amusement park	aquarium	Ave.	cat	dog	Ave.
OC-SVM	0.880	0.800	0.865	0.630	0.650	0.765	0.899	0.750	0.824
SO-Ours	0.928	0.936	0.948	0.837	0.900	0.910	0.984	0.943	0.964
SS-Ours	0.986	0.987	0.986	0.967	0.989	0.983	0.993	0.996	0.994
OC-NN	0.918	0.928	0.910	0.818	0.900	0.895	0.979	0.882	0.931
Deep A.Det.	0.824	0.735	0.798	0.604	0.647	0.722	0.883	0.892	0.888
DSEBM	0.676	0.630	0.633	0.462	0.662	0.613	0.460	0.571	0.516
DAGMM	0.660	0.520	0.548	0.547	0.374	0.530	0.498	0.472	0.485
AD-GAN	0.382	0.601	0.618	0.462	0.430	0.499	0.548	0.519	0.534

Table 6: AUROC scores for one-class detection task on each class of various datasets using different models. SO and SS implemented with understanding of hierarchical-models is competitive with recent deep-learned models across a wide range of tasks and features, with SS being almost always the best.

our *shell based learning* on the clustering problem that is worth further exporing in the next paper.

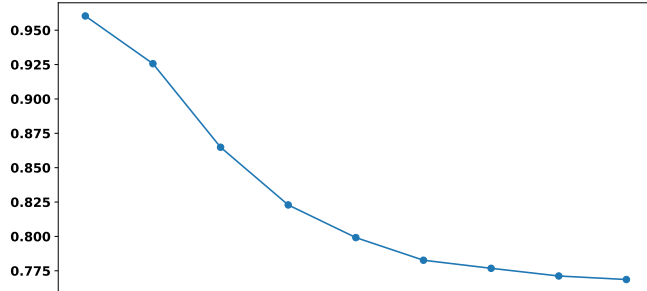


Figure 8: Average AUROC score on STL-10 dataset using ResNet [21] and OC-SVM [9]. Observe that much of the magically good performance of ResNet [21] derives from its choice of coordinate frame. Shifting the mean from origin causes a steady detotriation in results.

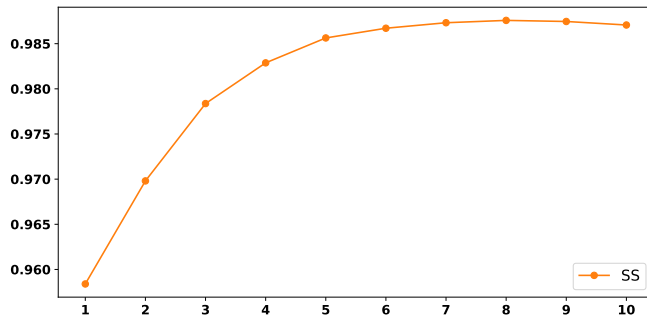


Figure 9: AUROC score on STL-10 dataset for Shells-Stacked (SS) with increasing number of shells. This demonstrates its ability to leverage external information.

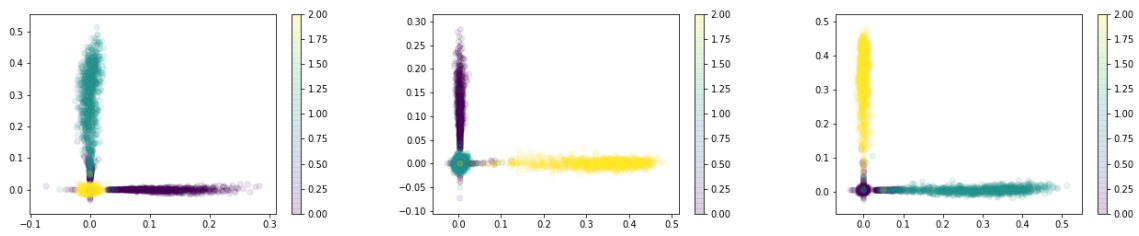


Figure 10: Shell based clustering result: x-axis and y-axis value in the plot represents the distance of a data point to the corresponding distinctive shell. From left to right: cat-vs-panda, dog-vs-cat and panda-vs-dog.